Flexural strength of post-tensioned concrete-filled fiber-reinforced-polymer rectangular tube beams

Asmaa Abdeldaim Ahmed, Mohamed Hassan, Radhouane Masmoudi, and M.-Iqbal Khan

The long-term durability of reinforced and prestressed concrete structures has become a major concern in the construction industry. Many bridges in Canada and the United States are approaching the end of their design life, and some bridges are showing major signs of structural damage, such as severe corrosion of steel bars and large cracks, due to their high level of exposure to environmental factors. In 2021, the American Society of Civil Engineers[1] reported that more than 42% of the bridges currently in use in Canada and the United States were built more than 50 years ago and a significant number of these structures need strengthening, rehabilitation, or replacement.

Hybrid members such as concrete-filled fiber-reinforced-polymer tubes (CFFTs) provide an effective system for many special types of structural applications, such as bridge piers, piles, and girders. The CFFT system offers an excellent alternative to conventional reinforced concrete or steel components in corrosive environments, especially tidal zones and splash zones for highway accoutrements where deicing salts are used. Although the system has proved to be practical and durable, the relatively low flexural stiffness of the system after cracking, which results in large deflections under service loads, presents an ongoing challenge. One way to address this challenge is to introduce longitudinal prestressing, which activates the confinement mechanism induced by the tube and considerably enhances the flexural strength and stiffness.[2–5]

Very little experimental data pertaining to the flexural behavior of prestressed CFFTs have been published.[2–5] Fam

■ This paper presents results of a research program to design and assess the potential use of concrete-filled fiber-reinforced-polymer beams post-tensioned with steel tendons in bridge applications.

■ The structural performance of five rectangular beams post-tensioned with steel tendons was evaluated. Test specimen configurations included one thin carbon-fiber-reinforced polymer laminate embedded in the tension flange to enhance flexural behavior, two thin carbon-fiber-reinforced polymer laminate strips embedded in the tension flange to enhance flexural behavior, and a double-inclined fiber pattern for the tube along the longitudinal direction.

■ This research provides a step toward constructing high-performance hybrid structural members for bridge applications.

and Mandal[2] investigated the flexural behavior of prestressed CFFTs. They found that the prestressing can improve the strength and serviceability of the system. ElGawady et al.[6] investigated the behavior of four hybrid segmental columns consisting of precast, post-tensioned CFFTs under lateral cyclic loading. The test results showed that these CFFTs were an effective system to resist lateral cyclic loads. The post-tensioned CFFT columns could undergo large nonlinear lateral deformations without experiencing significant or sudden loss of capacity. Recently, Ahmed et al.[3–5] tested 10 full-scale post-tensioned CFFT beams under flexural loading with a wide range of investigated parameters, such as concrete compressive strength, prestressing level and ratio, tube thickness, and loading scheme (static and cyclic). This study confirmed the effectiveness and feasibility of prestressing on the flexural behavior of rectangular CFFT beams tested in flexure.

The experimental work presented in this paper extends an extensive research program carried out at the University of Sherbrooke in Sherbrooke, QC, Canada, to design and assess the potential use of CFFT beams post-tensioned with steel tendons in bridge applications. In the investigation described in this paper, we evaluated the structural performance of five rectangular CFFT beams post-tensioned with steel tendons. Specifically, we tested the following up to failure:

- one post-tensioned CFFT beam attached with one thin carbon-fiber-reinforced-polymer (CFRP) laminate embedded in the tension flange to enhance the beam's flexural behavior

- one post-tensioned CFFT beam attached with two thin CFRP laminates embedded in the tension flange to enhance the beam's flexural behavior

- one post-tensioned CFFT beam with a double-inclined fiber pattern for the tube along the longitudinal direction

- two previously tested post-tensioned CFFT beams, which served as a reference for comparisons[5]

The effects of attaching a thin CFRP laminate embedded in the tension flange and its reinforcement ratio as well as the structural fiber pattern of the tube were investigated. Last, we propose a simplified design approach based on strain combinability and force equilibrium to estimate the flexural capacity of the tested beams. This research provides a step toward constructing high-performance hybrid structural members for bridge applications.

Materials

Concrete

Normal-strength concrete with a maximum aggregate size of 14 mm (0.55 in.) was used to cast the test specimens. The development of concrete strength with age was monitored per ASTM C397 using three 100×200 mm (3.94×7.87 in.) concrete cylinders tested at 7, 14, and 28 days. On the day of testing, six cylinders (100×200 mm) were tested to determine the characteristics of the concrete under compression and tension tests. **Table 1** reports the concrete characteristics of each specimen.

Steel

Investigators used 15.2 mm (0.6 in.) diameter seven-wire strand for prestressing. The steel reinforcing bars used as bonded reinforcement at the bottom side and steel stirrups of the test specimens were 15M (no. 5), which has a 16 mm (0.63 in.) nominal diameter, and 10M (no. 3), respectively.

The material characteristics of steel strands and reinforcing bars for each diameter were obtained as per ASTM A615[8]

Table 1. Details of test specimens

Beam	$B_i \times H_i$	Tube type	t_f, mm	Prestressing Number of strands	Prestressing P_j, kN	Prestressing P_{eff}, kN	Steel reinforcing bars	CFRP sheet	f_c', MPa	f_t' MPa
P_1-C		C	6.00		200	169		n/a	46 ± 0.9	4.0 ± 0.2
P_2-D		D	10.1		201	170		n/a	43 ± 0.7	3.8 ± 0.3
P_3-B	305 × 406 mm	B	7.40	Two 15.2 mm	200	171	Two 15M	n/a	46 ± 0.9	4.0 ± 0.2
P_4-B-C1		B	7.40		199	172		1 S1512	43 ± 0.7	3.8 ± 0.3
P_5-B-C2		B	7.40		200	170		2 S1512	43 ± 0.7	3.8 ± 0.3

Note: n/a = not applicable; B_i = inner tube width; CFRP = carbon-fiber-reinforced polymer; f_c' = cylinder unconfined concrete compressive strength; f_t' = cylinder tensile concrete strength; GFRP, glass-fiber-reinforced polymer; H_i = inner tube height; CFRP = carbon-fiber-reinforced polymer; GFRP = glass-fiber-reinforced precast concrete; n/a = not applicable; P_{eff} = effective prestressing forces at transfer; P_j = jacking force; P_1-C = prestressing beam with GFRP tube type C lateral reinforcement; P_2-D = prestressing beam with GFRP tube type D lateral reinforcement; P_3-B = prestressing beam with GFRP tube type B lateral reinforcement; P_4-B-C1 = prestressing beam with GFRP tube type B lateral reinforcement with one tensioned CFRP strip; P_5-B-C2 = prestressing beam with GFRP tube type B lateral reinforcement with two tensioned CFRP strips; t_f = tube thickness. 15M = no. 5; 1 mm = 0.0394 in.; 1 kN = 0.225 kip; 1 MPa = 0.145 ksi.

based on testing five samples. **Table 2** provides the material characteristics of steel strands and reinforcing bars.

Carbon-fiber-reinforced polymer strips

A 150 mm (5.9 in.) wide high-modulus pultruded unidirectional carbon fiber fabric was embedded between the fiber laminates at the tension side of the tube during its fabrication to improve the flexural behavior of the tested beams. After the first fiber layer was completed, the machine was stopped so that the carbon strip could be installed within the tube's fiber laminate. A vinyl ester resin layer was applied on one side of the strip surface, then another layer of resin was applied to the other side after the strip was attached to the tube. Continuous hand pressure with a roller was used to ensure there were no voids between the strip and the tube. The CFRP composite laminate was 1.2 mm (0.047 in.) thick, and according to the manufacturer's data, the ultimate tensile stress of the CFRP strips f_{fu}, the modulus of elasticity of the CFRP strips E_{fu}, and the ultimate tensile strain of the CFRP strips ε_{fu} were 2.8 GPa (406 ksi), 165 GPa (23,931 ksi), and 1.7%, respectively.

Glass-fiber-reinforced polymer tubes

The glass-fiber-reinforced polymer (GFRP) tubes were fabricated using the filament-winding manufacturing process. Three types of tubes (types B, C, and D) were used in this study. The GFRP tubes were manufactured using E-glass fibers wetted in vinyl ester with different amounts of roving and structural fiber laminates. Types B and C had the same stacking sequence (90 degrees, ±30 degrees, 90 degrees) but different amounts of fiber roving. Final tube thicknesses were 7.40 mm (0.29 in.) for type B and 6.0 mm (0.24 in.) for type C. Tube type D had the same amount of roving as type C, but the inclined fiber pattern along the longitudinal direction was repeated twice for type D and the type D stacking sequence was 90 degrees, ±30 degrees, ±30 degrees, 90 degrees. The final wall thickness of tube D was 10.1 mm (0.40 in.). Tension and compression material characteristics in the axial and hoop directions were obtained from testing four coupons per ASTM D3039[9] and ASTM D695.[10] **Table 3** lists the material characteristics of all tubes. **Figure 1** depicts the behavior of GFRP coupons in the axial direction and the coupons test setup, and **Fig. 2** shows tube fabrication using the filament winding technique.

Table 2. Mechanical properties of steel strands and reinforcing bars						
Reinforcement type	Nominal diameter, mm	Nominal area, mm²	E_s or E_p, GPa	f_y or f_{py}, MPa	f_u or f_{pu}, MPa	ε_y or ε_{py}, %
15 mm (strand)	15.2	140	197.8 ± 0.9	1802 ± 30.0	1967 ± 22.0	0.01 ± 0.06
10M (deformed)	11.3	100	200.4 ± 0.6	420 ± 20.0	610 ± 40.0	0.21 ± 0.07
15M (deformed)	16.0	200	199.9 ± 0.5	460 ± 10.0	620 ± 30.0	0.24 ± 0.09

Note: E_p = elastic modulus of prestressing strand; E_s = elastic modulus of steel bar; f_{pu} = ultimate tensile stress of prestressing strands; f_{py} = yield tensile stress of strands; f_u = ultimate tensile stress of the steel bars; f_y = yield tensile stress of steel bars; ε_{py} = yield strain of strand; ε_y = yield strain of steel bar. 10M = no. 3; 15M = no. 5; 1 mm = 0.0394 in.; 1 mm² = 0.00155 in.²; 1 MPa = 0.145 ksi; 1 GPa = 145 ksi.

Table 3. Mechanical properties of glass-fiber-reinforced-polymer tubes in longitudinal and transverse directions									
Tube type	t_f, mm	Stacking sequence,* degree	Test direction	Tensile coupon test†			Compression coupon test*		
				$f_{ft,ave}$, MPa	$E_{ft,ave}$, GPa	$\varepsilon_{ft,ave}$, %	$F_{fc,ave}$, MPa	$E_{fc,ave}$, GPa	$\varepsilon_{fc,ave}$, %
B	7.40	90, ±30, 90	Longitudinal (axial) direction	107.5 ± 11.1	12.7 ± 0.83	1.38 ± 0.15	137.3 ± 16.1	15.0 ± 2.11	1.65 ± 0.31
C	6.00	90, ±30, 90		115.4 ± 5.5	13.0 ± 0.82	1.41 ± 0.09	126.0 ± 2.6	13.1 ± 1.93	1.84 ± 0.24
D	10.1	90, ±30, ±30, 90		163.3 ± 5.2	15.7 ± 2.44	1.33 ± 0.20	134.4 ± 4.4	13.1 ± 0.76	1.62 ± 0.36
B	7.40	90, ±30, 90	Transverse (hoop) direction	344.2 ± 27.3	15.7 ± 2.90	2.60 ± 0.44	319.3 ± 14.1	18.9 ± 0.85	2.91 ± 0.18
C	6.00	90, 30, 90		318.8 ± 23.2	15.5 ± 1.00	2.60 ± 0.45	312.5 ± 21.8	17.5 ± 1.26	2.24 ± 0.24
D	10.1	90, ±30, ±30, 90]		268.6 ± 10.1	14.8 ± 0.61	2.95 ± 0.29	232.7 ± 4.70	12.7 ± 0.41	2.83 ± 0.42

Note: $E_{fc,ave}$ = elastic modulus of tube from compression coupon test; $E_{ft,ave}$ = tensile elastic modulus of tube from tensile coupon test; $f_{fc,ave}$ = compression strength of the tube from compression coupon test; $f_{ft,ave}$ = tensile strength of the tube from tensile coupon test; t_f = tube thickness; $\varepsilon_{ft,ave}$ = tensile strain of tube from tensile coupon test; $\varepsilon_{fc,ave}$ = compression strain of tube from compression coupon test. 1 mm = 0.0394 in.; 1 MPa = 0.145 ksi; 1 GPa = 145 ksi.
*Average values of flange and web directions.
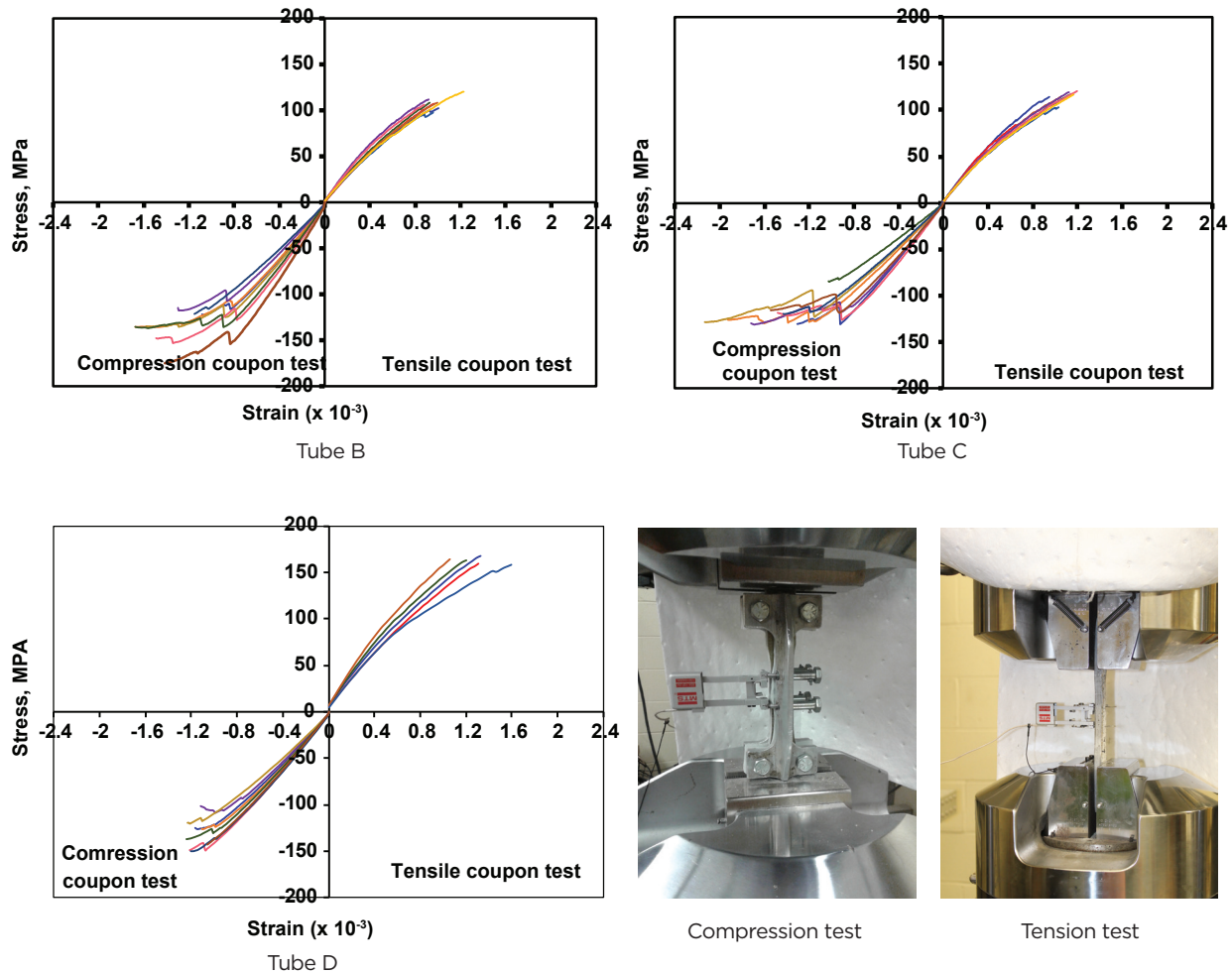†Angles measured with respect to longitudinal axis of tube.

Figure 1. Behavior of glass-fiber-reinforced polymer coupons in axial direction. Note: 1 MPa = 0.145 ksi.

Test specimen details

Table 1 provides details for the five rectangular full-scale post-tensioned CFFT beams that were constructed and tested up to failure. Beam specimens are identified in the format $P_{(No.)}$-x-y, where $P_{(No.)}$ is the prestressing beam label; x is the lateral reinforcement type (B is GFRP tube type B, C is GFRP tube type C, and D is GFRP tube type D), and y is the number of tensioned CFRP strips, if any (C1 is one strip and C2 is two strips). Specimens P_3-B-C1 and P_5-B-C2 were designed to investigate the effect of attaching one or two thin CFRP laminates embedded in the tension flange; their behavior was compared with the behavior of their counterpart reference specimen, P_4-B, which did not have a CFRP strip. Specimens P_1-C and P_2-D were used to investigate how doubling the inclined fiber pattern for the tube along the longitudinal direction affected the beam's flexural behavior at the same amount of roving.

All beam specimens were 305 mm wide × 406 mm deep (12 × 16 in.) and had a span length of 3300 mm (129.9 in.). Two 15M (no. 5) steel bars were used at the tension side of the

beams as bonded reinforcement per CSA A23.3.[11] At both of the end anchorage zones for each post-tensioned CFFT, 10M (no. 3) steel stirrups placed 100 mm (3.94 in.) apart were used to properly confine the concrete and avoid any occurrence of failure. All prestressing tendons were at the same eccentricity e of 85 mm (3.35 in.). The eccentricity was measured from the inner bottom surface of the FRP tube to the center of the tendon duct. The eccentricity of tendons was designed to only permissible tensile stresses in concrete immediately after prestressing transfer not exceed tensile stress of $0.5\sqrt{f_c'}$ per CSA A23.3[11], where f_c' is unconfined concrete compressive strength. All prestressed beams were tensioned up to 65% f_{pu}, where f_{pu} is the ultimate tensile stress of the steel strands. Table 1 lists the jacking forces P_j as well as the effective prestressing forces at transfer P_{eff} for each tendon. **Figure 3** shows the test specimens' details.

Specimen preparation

FRP tubes were used as a stay-in-place formwork to cast the test specimens. To improve the bond between the concrete and

Filament winding machine

Beam casting setup and casting

Figure 2. Photographs of beam production setup.

tube, the entire length of the beam inner surface was wetted with vinyl ester resin and then coated with coarse sand particles. Steel cages were assembled and placed inside the tubes (Fig. 3). The whole assembly was then carefully positioned over a steel bed. An inclined steel bed was designed to allow the concrete to consolidate under its own weight. Although an inclined framework system was used to cast 13 m [43 ft] long precast concrete piles using CFFTs for a Route 40 bridge in Virginia,[12] for example, casting concrete in an inclined framework may be costly, which may limit the size of the beams. The tubes were closed at one end with wood and sealed around the tube to fill any voids. The concrete was cast using a pump from the other end and vibrated internally with a vibrator to avoid any concrete segregation. After filling the tube, the top opening was properly closed with plywood. The CFFTs were cured inside the lab for about 50 days before testing. Figure 2 shows the beam on the casting setup.

Instrumentation

The deflection of the test specimens at different locations was captured using five 250 mm (9.84 in.) long string potentiometers. Two other 250 mm long string potentiometers measured the axial strains at the top and bottom surfaces at midspan. The slippage between the concrete and the FRP tube at both ends was captured using two 25 mm (0.98 in.) string potentiometers. To monitor the prestressing forces during the test, two load cells were placed at the dead end of each tendon. **Figure 4** shows the locations of different instruments. Each beam was equipped with 22 strain gauges (6 mm [0.24 in.] in length) at the midspan that were glued over the outer surface of the tubes in the axial and transverse directions. In addition, two other strain gauges were attached before casting over the steel reinforcing bars at the midspan. Prestressing tendons were also mounted with four strain gauges at -350, 0, +350, and +575 mm (-13.78, 0, 13.78,

Polyvinyl chloride ducts and steel cages
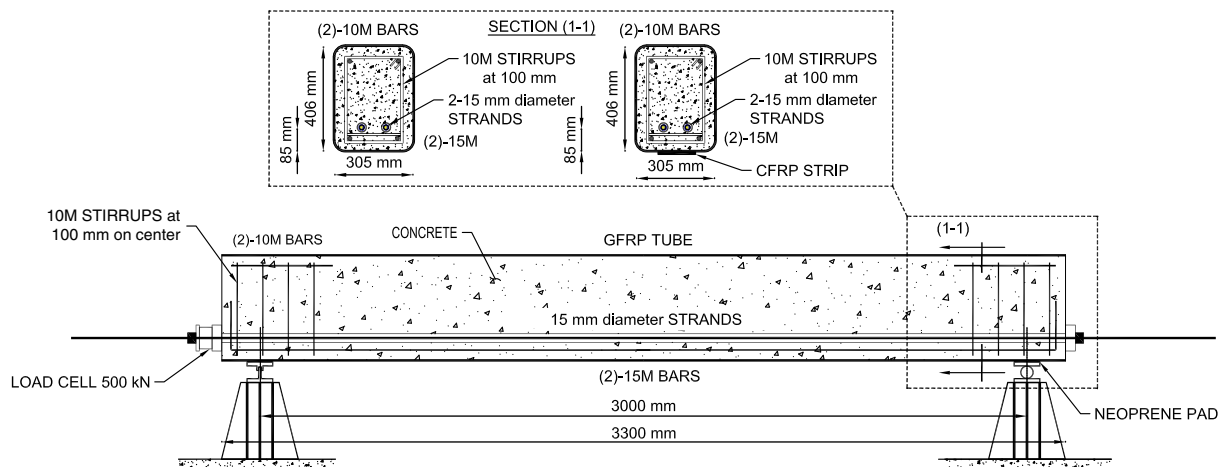
Post-tensioned concrete-filled fiber-reinforced polymer tube beam

Figure 3. Beam geometry and reinforcement details. Note: CFRP = carbon-fiber-reinforced polymer; GFRP = glass-fiber-reinforced polymer. 10M = no. 3; 15M = no. 5; 1 mm = 0.0394 in.; 1 kN = 0.225 kip.

and +22.64 in.) distance from the beam's centerline. All sensors were attached to a data acquisition system to record all data.

Test setup

Figure 5 depicts the test and prestressing frame setups. Flexural load tests were conducted using a four-point loading setup. The beams were simply supported with a hinge and roller system. The distance between the end supports was 3000 mm (118.11 in.), and the constant moment region distance was 700 mm (27.56 in.). All beams were tested using a 10,000 kN (2248 kip) load testing machine at a displacement-controlled rate of 1 mm/min (0.039 in./min) through two loading points on the test beam. All tendons were post-tensioned in ungrouted ducts. Steel strands were anchored at one end using chuck anchors and end bearing steel plates. The strands were tensioned from the live end using a manual jack on each strand and were anchored using another set of chucks and bearing plates. Prestressing forces were applied gradually up to the desired prestressing force. The jacking force was monitored during the test using a load cell of 500 kN (112.4 kip) installed at the dead

end of each strand and verified by the strain gauges on the steel strands. Table 1 reports the jacking prestressing force P_j and the effective prestressing forces at transfer P_{eff}.

Test results

Mode of failure

Generally, the resin matrix started to crack and was followed by compression buckling of the tube between the two-point loading in the constant moment region. The concrete in the compression zone was highly compressed due to the load increases and excessively expanded in the hoop direction until the fibers were fractured. The fracture of the fibers was later extended into the beam depth at both sides. Loading of the specimens was continued until the post-tensioned CFFT beams failed by tube fracturing in the tension side. After the tube ruptured, the load was decreased to about two-thirds of the ultimate load and then the load-deformation curve was stabilized over an ample range of deformation. This behavior is similar to that of non-post-tensioned CFFT rectangular tubes tested under flex-
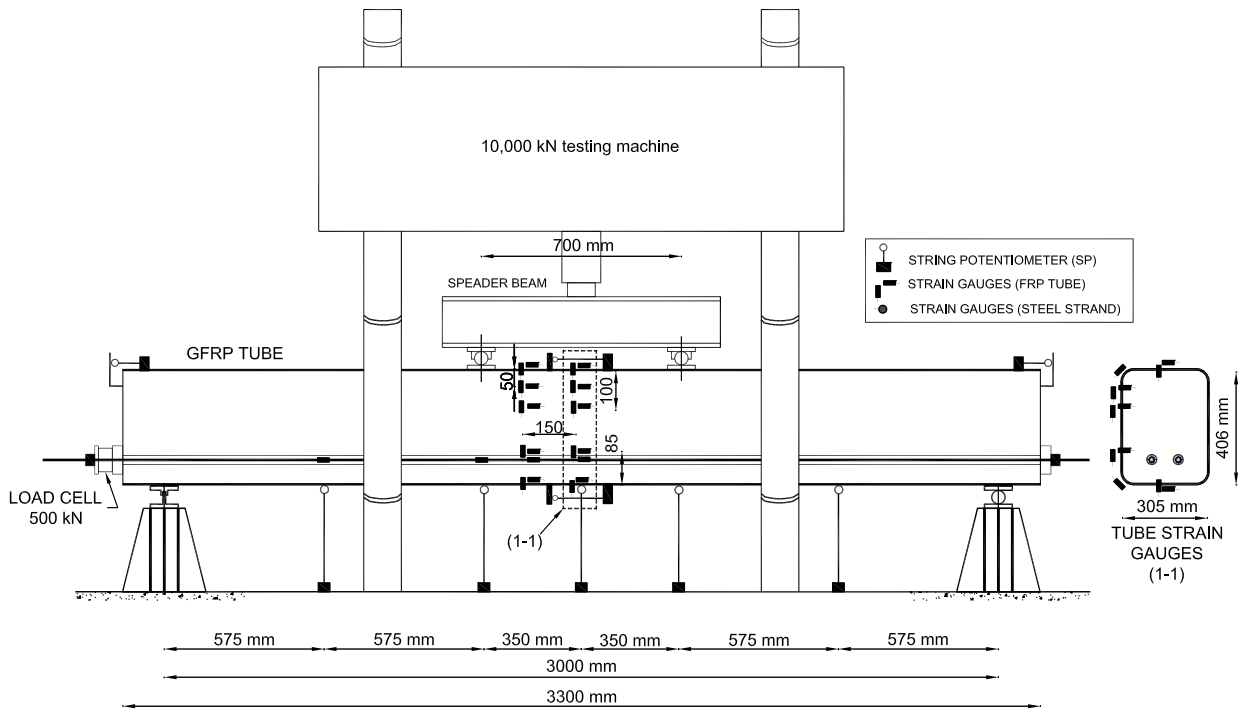
Figure 4. Instrumentation layout. Note: FRP = fiber-reinforced polymer; GFRP = glass-fiber-reinforced polymer. 1 mm = 0.039 in.; 1 kN = 0.225 kip.

Table 4. Summary of test results and ultimate flexural moment capacity predictions

Specimen	P_{cr}, kN	P_y, kN	P_u, kN	M_{cr}, kN-m	M_y, kN-m	M_u, kN-m	Δ_{cr}, mm	Δ_y, mm
P₁-C	173	365	804	99	210	462	2.10	11.5
P₂-D	198	422	1130	114	243	650	2.44	10.7
P₃-B	189	355	953	109	204	548	2.16	9.2
P₄-B-C1	206	419	1089	118	241	626	1.84	9.8
P₅-B-C2	210	445	1128	121	256	649	3.47	11.6
Average	n/a	n/a	n/a	n/a	n/a	n/a	n/a	n/a
Standard deviation	n/a	n/a	n/a	n/a	n/a	n/a	n/a	n/a
COV, %	n/a	n/a	n/a	n/a	n/a	n/a	n/a	n/a

Note: COV = coefficient of variation; $E_{elastic}$ = elastic energy absorption; E_{tot} = total energy absorption; M_{cr} = cracking moment; M_{pred} = predicted moment capacity; M_u = ultimate moment; $M_{u,exp}$ = ultimate moment from experimental test; M_y = yielding moment; P_{cr} = cracking load; P_u = peak load; P_y = yielding load; P₁-C = prestressing beam with GFRP tube type C lateral reinforcement; P₂-D = prestressing beam with GFRP tube type D lateral reinforcement; P₃-B = prestressing beam with GFRP tube type B lateral reinforcement; P₄-B-C1 = prestressing beam with GFRP tube type B lateral reinforcement with one tensioned CFRP strip; P₅-B-C2 = prestressing beam with GFRP tube type B lateral reinforcement with two tensioned CFRP strips; Δ_{cr} = deflection corresponding to cracking load; Δ_u = deflection corresponding to ultimate load; Δ_y = deflection corresponding to yielding load; ε_c = ultimate strain in compression surface; ε_t = ultimate strain in tension surface; λ = ductility factor; μ_p = energy ratio up to peak load. 1 mm = 0.0394 in; 1 kN = 0.2248 kip; 1 kN-m = 8.86 kip.in.
*Proposed model using unconfined concrete model.
†Proposed model using partially confined concrete model

ural loading.[13–15] **Figure 6** depicts the mode of failure of each beam after testing. It should be noted that the post-tensioned CFFT specimens (P$_4$-B-C1 and P$_5$-B-C2) with CFRP laminates showed a progressive failure at a high load level. The failure was initiated by fracture of the GFRP tube flange and then the CFRP laminate. It appears that once the CFRP was fractured at such a high load level, the beams failed. This behavior likely occurred because the CFRP strips were embedded inside the GFRP tube tension flange, which provided some warning before failure. By comparison, progressive failure was not observed in a case study by Fam and Skutezky[16] in which the CFRP laminate was bonded at the external tensioned flange.

After testing, the FRP tube was cut and removed so investigators could examine the condition of the concrete (Fig. 6). Like typical post-tensioned concrete beams, post-tensioned CFFT beams exhibited many flexural cracks close together near the midspan with a concrete crushing in the compression zone. Investigators also observed that the number of cracks at the tension side of the concrete was increased when the CFRP laminate was attached in the tension flange and the number of layers of the tube in the hoop direction was increased from one to two such as in specimen P$_2$-D.

Load-deflection relationships

Figure 7 shows the load–midspan deflection curves for all beams. **Table 4** reports the test results of all tested beams. The loads due to cracking and yielding were determined from the strain gauges on the bottom steel bars. Generally, the load-deflection responses for the post-tensioned CFFT beams

showed an almost trilinear response. The first slope represents the precracking stage up to concrete cracking, the second slope represents a reduced stiffness (preyielding stage), and the third slope represents the postyielding nonlinear stage with strength hardening. The nonlinear behavior was due to the relatively nonlinear stress-strain responses of the GFRP tubes, as evident from the coupon test results and the nonlinear characteristics of the concrete fill. The stiffness of test specimens decreased after the initiation of concrete cracking (Fig. 7). However, the ultimate loads were highly improved by attaching the CFRP laminates on the tension side and increasing the tube's structural fiber laminate from one layer to two. Specimens P$_1$-C, P$_2$-D, P$_3$-B, P$_4$-B-C1, and P$_5$-B-C2 failed, respectively, at 804, 1130, 953, 1089, and 1128 kN (181, 254, 214, 245, and 254 kip) ultimate loads at 95.9, 97.0, 97.4, 91.1, and 96.9 mm (3.78, 3.82, 3.84, 3.59, and 3.82 in.) corresponding to ultimate deformations.

Load-strain relationships

Figure 8 depicts the load–strain curves for all specimens at the midspan. The post-tensioned CFFT beams P$_1$-C, P$_2$-D-2, P$_3$-B, P$_4$-B-C1, and P$_5$-B-C2 failed in flexure by fracture of the tube in the tension side at 16,930, 18,264, 14,050, 12,894, and 12,137 με ultimate tensile strains, respectively (Fig. 8). These strains were more consistent with those measured from tensile coupon tests (Table 3). The ultimate longitudinal compressive strains for specimens P$_1$-C, P$_2$-D-2, P$_3$-B, P$_4$-B-C1, and P$_5$-B-C2 were -4788, -7601, -7408, -5685, and -4396 με, which are 74%, 53%, 55%, 66%, and 73% of the measured strains from compressive coupon tests, respectively. The longitudi-

Table 4. (cont.)								
Δ_u, mm	ε_c, με	ε_t, με	Δ_u/Δ_y	$E_{elastic}$, kN-m	E_{tot}, kN-m	μ_p, %	$M_{u,exp}/M_{pred}$*	$M_{u,exp}/M_{pred}$†
95.9	-4788	16,930	8.3	7.2	57.7	88	1.13	1.04
97.0	-7601	18,264	9.1	16.8	118.3	86	1.15	1.13
97.4	-7408	14,050	10.6	10.3	68.1	85	1.19	1.06
91.1	-5685	12,894	9.3	14.4	110	87	1.06	1.04
96.9	-4396	12,137	8.4	16.1	88.9	82	1.01	1.00
n/a	n/a	n/a	n/a	n/a	n/a	n/a	1.11	1.05
n/a	n/a	n/a	n/a	n/a	n/a	n/a	0.07	0.05
n/a	n/a	n/a	n/a	n/a	n/a	n/a	6.5	4.5

Figure 5. Load test setup. Note: P = load. 1 mm = 0.0394 in.

nal compressive strains inverted their direction as the load increased (Fig. 8). This response indicates the start of the outward local compression buckling of the tube.[15] However, the tubes carried further loads until they ruptured in a flexural tension behavior.

Increasing the longitudinal flexural stiffness by attaching a thin CFRP laminate in tension flange as well as doubling

the inclined fiber laminate in the hoop direction significantly decreased the tubes and steel strand strains at the same load level. Figure 8 depicts the load–midspan hoop strain response of all specimens in the compression region. In general, the load–hoop strain curves show nearly a bilinear behavior with a first slope related to the tube's Poisson's ratio effect of 0.20. As the tube started to buckle locally, the concrete expanded excessively in the hoop direction, which
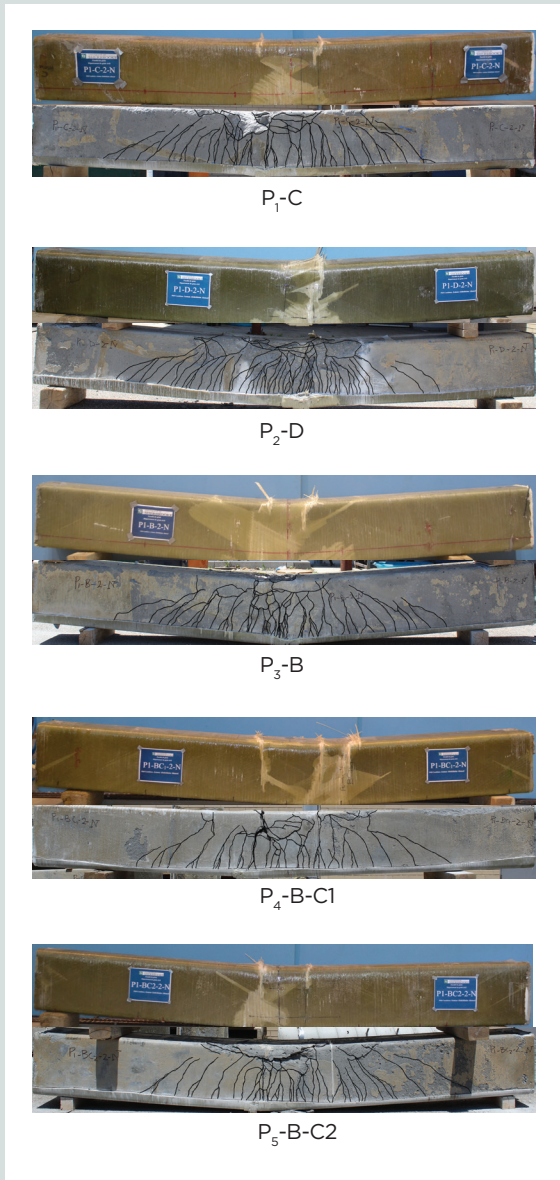
Figure 6. Failure mode of the tested beams and concrete crack patterns after removing the glass-fiber-reinforced polymer tubes. Note: CFRP = carbon-fiber-reinforced polymer; GFRP = glass-fiber-reinforced precast concrete; P_1-C = prestressing beam with GFRP tube type C lateral reinforcement; P_2-D = prestressing beam with GFRP tube type D lateral reinforcement; P_3-B = prestressing beam with GFRP tube type B lateral reinforcement; P_4-B-C1 = prestressing beam with GFRP tube type B lateral reinforcement with one tensioned CFRP strip; P_5-B-C2 = prestressing beam with GFRP tube type B lateral reinforcement with two tensioned CFRP strips.

resulted in additional hoop tensile strains in the top flange. As such, the transverse tensile strains in the FRP tube increased faster. This behavior was similar to what was found in a previous investigation of rectangular CFFT beams by Abouzied and Masmoudi.[14] The transverse strains at ultimate load in this study were between 6573 and 8497 $\mu\varepsilon$. Thus, the GFRP tubes were activated to confine the concrete more as the load increased.
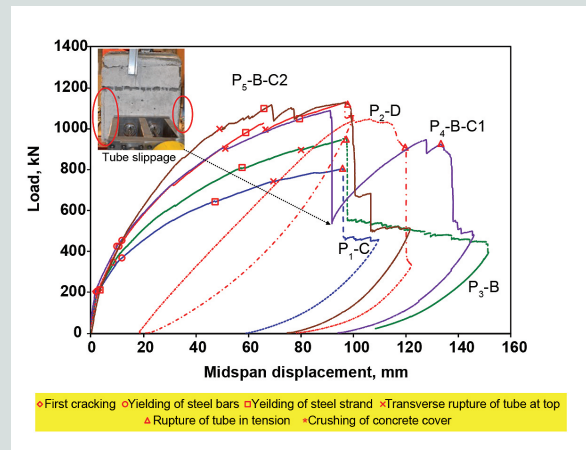

Figure 7. Load-deflection responses of the tested beams. Note: CFRP = carbon-fiber-reinforced polymer; GFRP = glass-fiber-reinforced precast concrete; P_1-C = prestressing beam with GFRP tube type C lateral reinforcement; P_2-D = prestressing beam with GFRP tube type D lateral reinforcement; P_3-B = prestressing beam with GFRP tube type B lateral reinforcement; P_4-B-C1 = prestressing beam with GFRP tube type B lateral reinforcement with one tensioned CFRP strip; P_5-B-C2 = prestressing beam with GFRP tube type B lateral reinforcement with two tensioned CFRP strips. 1 mm = 0.0394 in.; 1 kN = 0.225 kip.

Progression of neutral axis depth

Figure 9 illustrates the progression of the neutral axis depth ratio c/H with the load for all CFFTs, where c is the neutral axis depth and H is the beam total depth. The neutral axes were determined from the maximum recorded strains on the compression and tension surfaces of the tested beams. After cracking, the neutral axis depth shifted toward the compression zone to balance the tensile internal forces on the cross section. The position of the neutral axis depths after cracking initially decreased and later stabilized at a depth of 30% to 42% of the total depth of the section. When the concrete was examined after the tube was removed, investigators noticed a distinct compression zone along the length of the beams (Fig. 6). This observation is consistent with findings from the previous studies by Fam and Rizkalla[17] and Idris and Ozbakkaloglu.[18] It should be noted that the c/H ratio was slightly higher than the observed values reported by Helmi et al[12] and Abouzied and Masmoudi[13] for non-post-tensioned rectangular CFFT beams, which ranged from 20% to 30%.

Load-slip relationships

Figure 10 shows the relative slip between the tube and concrete at dead and live ends. There was a negligible relative slip between the FRP tube and concrete throughout the test at both ends up to the ultimate load. For specimen P_5-B-C1, the maximum recorded values at ultimate load were 0.22 and 1.12 mm (0.009 and 0.044 in.) at the dead and live ends, respectively. This finding confirms the full composite action between the tube and the concrete core. This behavior could be due to en-
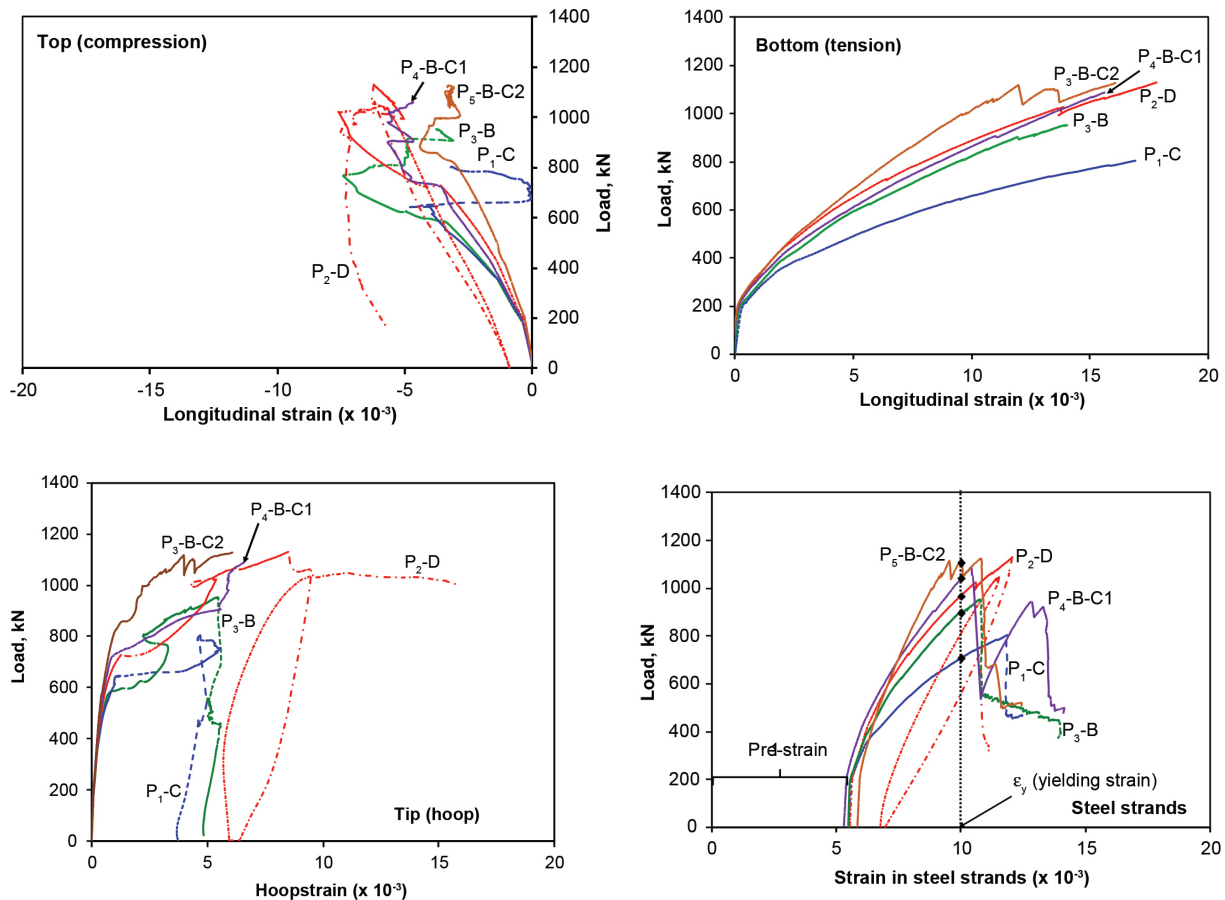
Figure 8. Load-strain responses of the fiber-reinforced polymer tubes and steel strands. Note: CFRP = carbon-fiber-reinforced polymer; GFRP = glass-fiber-reinforced precast concrete; P₁-C = prestressing beam with GFRP tube type C lateral reinforcement; P₂-D = prestressing beam with GFRP tube type D lateral reinforcement; P₃-B = prestressing beam with GFRP tube type B lateral reinforcement; P₄-B-C1 = prestressing beam with GFRP tube type B lateral reinforcement with one tensioned CFRP strip; P₅-B-C2 = prestressing beam with GFRP tube type B lateral reinforcement with two tensioned CFRP strips. 1 mm = 0.0394 in.; 1 kN = 0.225 kip.

hancement of the concrete confinement by the tube as a result of prestressing; also, the high frictional stresses developed at this interface resulted from the roughness of the inner surface of the tubes, which minimized the relative slip between the tube and concrete.[2,18] It should be mentioned that specimen P₅-B-C1 exhibited an initiation of relative slippage beyond 85% of the ultimate load. At the ultimate load, an audible noise occurred, with a remarkable reduction in the beam load and separation of the tube from the live end of the beam; however, no tube slippage was observed at the dead end. Although beam P₅-B-C1 exhibited an interface slip from the live-end side, the beam recovered its load until the beam fractured in the tension side.

Discussion

Effect of GFRP tube structural fiber pattern

To examine the effect of the tube structural fiber pattern, specimens P₁-C and P₂-D were manufactured using the

same amount of roving, but P₂-D had two layers in the inclined fiber pattern in the hoop direction. Figure 7 depicts the load-deflection behavior of the post-tensioned CFFT specimens. It can be observed from Fig. 7 that increasing the number of layers in the inclined fiber pattern in the hoop direction from one to two significantly improved the flexural strength and the post-peak behavior of the post-tensioned specimen P₂-D. In addition, it enhanced the serviceability requirements of specimen P₂-D substantially. This indicates that the flexural behavior is highly sensitive to the amount of inclined fiber laminate in the hoop direction. At ultimate load, the ultimate moment capacity of the post-tensioned CFFT beam P₂-D was improved by 41% compared with beam P₁-C, which had only a single inclined fiber pattern in the hoop direction. This finding suggests that increasing the amount of inclined fiber laminates leads to more-efficient post-tensioned CFFT structural members. However, more experimental tests are needed to address different fiber orientations with respect to the hoop direction.
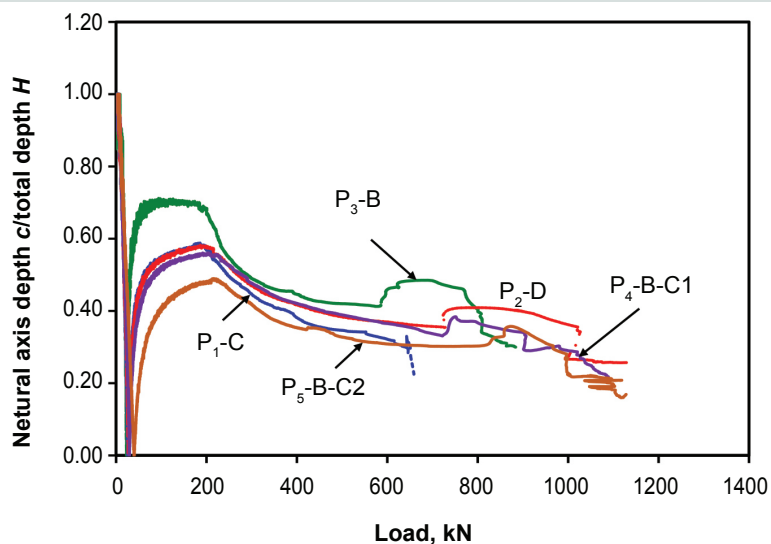
Figure 9. Variation of the neutral axis location as a function of the applied load. Note: CFRP = carbon-fiber-reinforced polymer; GFRP = glass-fiber-reinforced precast concrete; P₁-C = prestressing beam with GFRP tube type C lateral reinforcement; P₂-D = prestressing beam with GFRP tube type D lateral reinforcement; P₃-B = prestressing beam with GFRP tube type B lateral reinforcement; P₄-B-C1 = prestressing beam with GFRP tube type B lateral reinforcement with one tensioned CFRP strip; P₅-B-C2 = prestressing beam with GFRP tube type B lateral reinforcement with two tensioned CFRP strips. 1 mm = 0.0394 in.; 1 kN = 0.225 kip.

Effect of CFRP laminate in tension flange

To evaluate the effect of CFRP laminate in tension flange on the behavior and their total reinforcement ratio in the section, specimens P_3-B, P_4-B-C1, and P_5-B-C2 were compared (Fig. 7). Attaching the CFRP laminates embedded in the bottom GFRP flange resulted in 14% and 19% increases in flexural strength for specimen P_4-B-C1 (one CFRP laminate) and specimen P_5-B-C2 (two CFRP laminates), respectively (Fig. 7). This finding can be attributed to increases in the flexural stiffness due to the high elastic moduli of the CFRP laminate, which in turn substantially enhances the flexural strength. The test specimens exhibited similar stiffnesses before cracking. However, specimens P_4-B-C1 and P_5-B-C2 exhibited greater stiffness after cracking and lower deflection at a comparable load level compared with post-tensioned specimen P_3-B (no CFRP laminate). **Figure 11** presents the axial versus hoop strains in the compression side of all beams. The axial-transverse strain behavior of P_4-B-C1 and P_5-B-C2 showed a steeper shift in slope than that of beam P_3-B, which points out a higher confinement level. This finding is additionally confirmed by the fact that the respective transverse tensile strains in specimens P_4-B-C1 and P_5-B-C2 at failure were 6573 and 6082 με, respectively, which means those strains were respectively 22% and 13% higher than the transverse tensile strain in specimen P_3-B. The greater number of CFRP layers in specimen P_5-B-C2 only slightly affected the beam's flexural moment capacity and postcracking stiffness compared with P_4-B-C1. This finding may be explained by the small CFRP reinforcement ratio, which in turn had an insignificant impact on the flexural capacity.

Although tube type B was thinner than type D, it seems that with the attachment of the CFRP laminates in the bottom flange, the type B tube can achieve flexural strength and energy absorption comparable to that of type D, regardless of the fiber laminate in the hoop directions. This confirms the efficiency of both systems to enhance the flexural performance as well as the strength of the post-tensioned CFFT system.

Ductility index and energy absorption

Ductility is an important index for assessing the performance and safety of a concrete structure. Two methods were used in this study to examine the ductility of the tested beams in terms of deformation or energy absorption. In the first method, the ductility index λ can be expressed as follows[19]:

$$\lambda = \frac{\Delta_u}{\Delta_y}$$

where

Δ_u = midspan displacement at the ultimate state (corresponding to the peak of the load-carrying capacity)

Δ_y = midspan displacement at the first yielding of tension steel reinforcing bars

The ductility of post-tensioned members can be also evaluated by the ratio between the elastic and inelastic energies consumed under the load-deflection curve.[20–22] In this study, the ductility of the tested beams was based on the energy ratio up to peak load μ_p.[20]
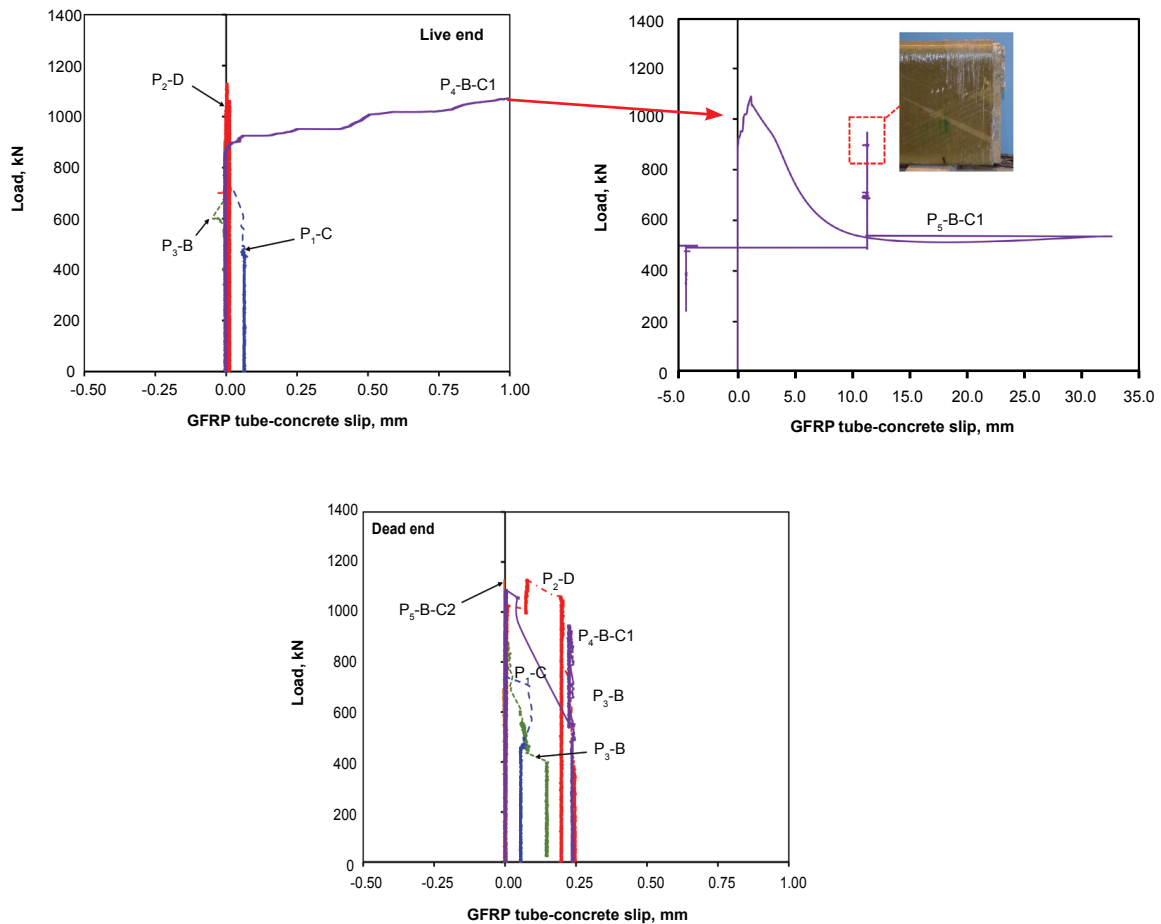
Figure 10. Load-slip relationships measured between fiber-reinforced polymer tube and concrete. Note: CFRP = carbon-fiber-reinforced polymer; GFRP = glass-fiber-reinforced precast concrete; P₁-C = prestressing beam with GFRP tube type C lateral reinforcement; P₂-D = prestressing beam with GFRP tube type D lateral reinforcement; P₃-B = prestressing beam with GFRP tube type B lateral reinforcement; P₄-B-C1 = prestressing beam with GFRP tube type B lateral reinforcement with one tensioned CFRP strip; P₅-B-C2 = prestressing beam with GFRP tube type B lateral reinforcement with two tensioned CFRP strips. 1 mm = 0.0394 in.; 1 kN = 0.225 kip.

$$\mu_p = \frac{E_{tot} - E_{elastic}}{E_{tot}}$$

where the total energy absorption E_{tot} is the area under the load-deflection curve and $E_{elastic}$ is elastic energy released upon failure, calculated as the area of the triangle formed at failure load by the line having the weighted average slope of the two initial straight lines of the load-deflection curve.[20] If the energy ratio is equal to or greater than 75%, the beam will exhibit a ductile failure. Beam behavior is considered semiductile if the energy ratio is between 70% and 74%. The beam may exhibit brittle failure if the energy ratio is equal to or less than 69%.[20] Table 4 summarizes the values of λ, calculated energy ratios of the tested beams, and total energy absorption. It shows that the estimated λ and μ_p values ranged, respectively, from 8.3 to 10.6 and 82% to 87% for the post-tensioned CFFT beams. This behavior is considered ductile and provides sufficient physical warning prior to failure. The test results also indicate that the total energy absorption was increased by providing CFRP lam-

inates in the tension flange and by increasing the number of fiber layers in the hoop direction from one to two. Compared with P₂-D, the total energy absorption increased by 105% and 74% for P₁-C and P₃-B, respectively. Furthermore, attaching CFRP laminates in the tension flange increased the total energy absorption by 62% for P₄-B-C1 (one laminate) and 31% for P₅-B-C2 (two laminates) compared with P₃-B.

Flexural moment capacity predictions

In this section, we present a simplified design approach based on strain combinability and force equilibrium to estimate the flexural moment capacity of the tested beams. In the model, we make several assumptions, such as the plane section remains plane after deformation, linear strain distribution along with the section depth, and a full bond between the tube and concrete. Linear elastic responses for the GFRP tube and CFRP laminate materials in compression and tension until rupture are determined from coupon tests. A bilinear model
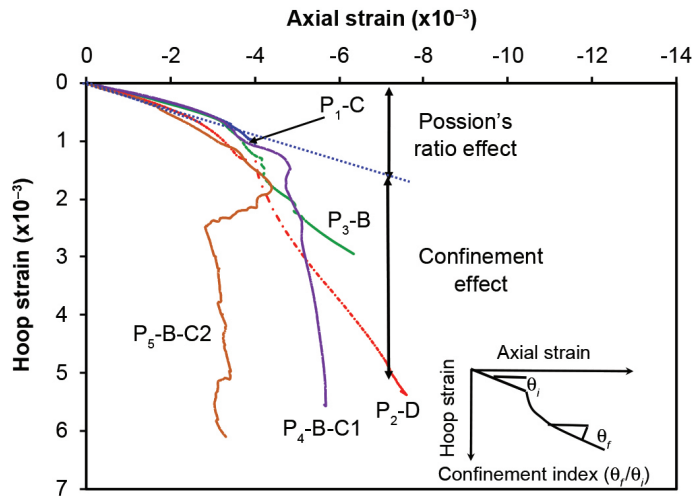
Figure 11. Axial versus hoop strain behavior. Note: CFRP = carbon-fiber-reinforced polymer; GFRP = glass-fiber-reinforced precast concrete; P₁-C = prestressing beam with GFRP tube type C lateral reinforcement; P₂-D = prestressing beam with GFRP tube type D lateral reinforcement; P₃-B = prestressing beam with GFRP tube type B lateral reinforcement; P₄-B-C1 = prestressing beam with GFRP tube type B lateral reinforcement with one tensioned CFRP strip; P₅-B-C2 = prestressing beam with GFRP tube type B lateral reinforcement with two tensioned CFRP strips; Θ_f = final slope of the axial-hoop strain curve; Θ_i = initial slope of the axial-hoop strain curve. 1 mm = 0.0394 in.; 1 kN = 0.225 kip.

is undertaken to model the steel bars, with a zero-plastic behavior after yield. The concrete on the tension side is ignored. Unconfined and partially confined models are considered herein to model the concrete in compression. The concrete in compression in the unconfined model displays elongated strain-softening using Popovics's model.[23] The partially confined model, which stipulates an intermediate level of confinement, is similar to Popovics's model[23] up to f'_c followed by a zero-slope relationship following Fam et al.[24]

$$f'_c = \frac{f'_c(\varepsilon_c / \varepsilon'_c)r}{r-1+(\varepsilon_c / \varepsilon'_c)^r}$$

$$f'_c = f'_{co} \text{ when } \varepsilon_c > \varepsilon'_c$$

where

r is constant $= E_{co}/(E_{co} - E_{sec})$ and the secant modulus of concrete $E_{sec} = f'_c / \varepsilon'_c$. The concrete module is computed as $E_{co} = 5000\sqrt{f'_c}$ and compression concrete cylinder strain at the ultimate load $= \varepsilon'_c = 0.0023$.

A modified Ramberg-Osgood function, proposed by Mattock,[25] was undertaken to model the stress and strain curve of strands as follows. **Figure 12** presents the concrete and strand proposed material models.

$$f_p = E_p\varepsilon_p\left(A + \frac{(1-A)}{\left[1+(B\varepsilon_p)^c\right]^{1/C}}\right) \le f_{pu}$$

where

E_p = elastic modulus of prestressing strands

ε_p = prestressing strain at any point on the strand stress-strain curve

A = constant

B = constant

c = neutral axis depth

C = constant

f_{pu} = ultimate stress of prestressing strands

The function consists of two straight lines joined by a curve and is defined by four constants E_p, A, B, and C. Knowing the values of E_p (197.8 GPa [28,687 ksi]), f_{pu} (1977 MPa [287 ksi]), and ε_{pu} (7.03%) from the experimental test results, the constants A, B, and C can be experimentally determined and the stress-strain relationship can be established (Fig. 12), which is given by the following equation:

$$f_p = 197,800\varepsilon_p\left(0.015 + \frac{0.985}{\left[1+(109.8\varepsilon_p)22\right]^{1/22}}\right)$$

$$\le 1967 \text{ MPa } (285 \text{ ksi})$$

where the constants A, B, and C are 0.015, 109.8, and 22, respectively

The model procedure began by assuming the bottom strain value $\varepsilon_{tube,bottom}$ of the tube from the tensile coupon tests and the compression zone depth c, assuming tension failure is governed by rupture of the tube in tension. The stresses along
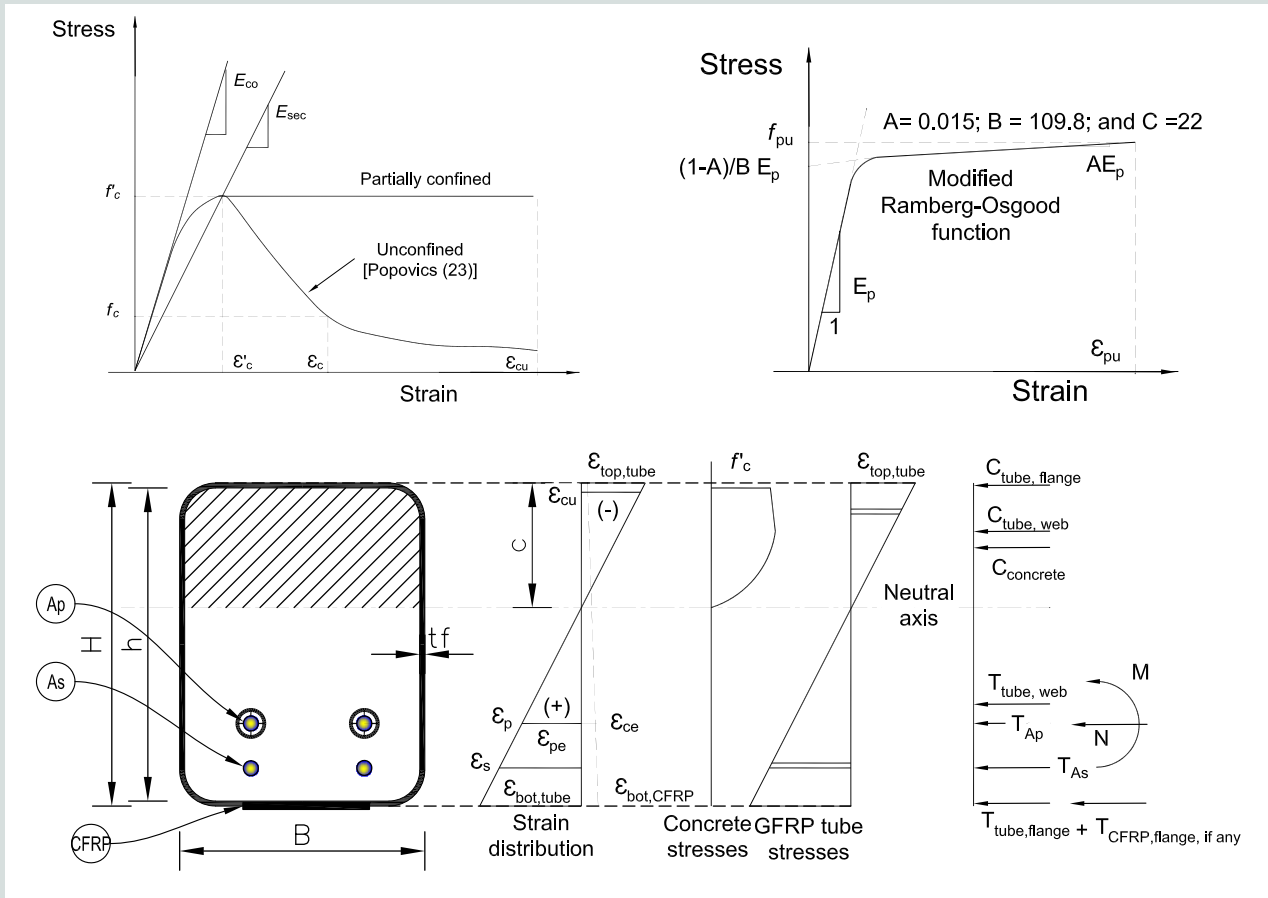
Figure 12. Stress-strain models. Note: A = constant; A_p = cross sectional area of prestressing strands; A_s = cross-sectional area of steel bars; B = constant; c = neutral axis depth; C = constant; $C_{concrete}$ = concrete compression force; $C_{tube,flange}$ = compression force of the tube in the compression flange; $C_{tube,web}$ = compression force of the tube web in the compression zone; CFRP = carbon-fiber-reinforced polymer; E_{co} = concrete modulus; E_p = elastic modulus of prestressing strands; E_{sec} = secant modulus of elasticity; f_c = concrete strength at any point of the stress-strain curve; f_c' = unconfined compressive strength of concrete cylinder; f_{pu} = ultimate stress of prestressing strand; GFRP = glass-fiber-reinforced polymer; h = inner tube depth; H = total depth; M = external moment; N = external apply forces; T_{Ap} = force at prestressing strands; T_{As} = force at steel bars; $T_{CFRP,flange}$ = force in the CFRP strips at the tension zone; t_f = tube thickness; $T_{tube,flange}$ = force in the tube flange at the tension zone; $T_{tube,web}$ = force in the tube web at the tension zone; $\varepsilon_{bot,CFRP}$ = strain in the CFRP strip; $\varepsilon_{bot,tube}$ = strain in the tube bottom side; ε_c =strain in the concrete; ε_c' = ultimate concrete strain at peak load; ε_{cu} = strain at concrete level; ε_p = strain at the prestressing strand level; ε_{pu} = ultimate strain of prestressing strands; ε_s = strain in the steel bars; $\varepsilon_{top,tube}$ = strain in the tube top side.

the cross section were computed from the corresponding strains. The internal forces were determined by multiplying the stress by the corresponding area of different materials. The equilibrium was then checked by achieving an acceptable tolerance between the summation of forces in compression and tension. When the equilibrium was fulfilled, the internal moments were computed by multiplying the internal forces by the distance from the neutral axis of the section. **Figure 12** presents the stress and strain distribution of the proposed theoretical model. Further details on the internal force computations can be found in the literature.[13,14]

Comparison of analytical experimental results

Figure 13 presents comparisons between the estimated values of the flexural strength and the test results using

different concrete models. The predicted values on the basis of the partially confined concrete model demonstrated an excellent agreement with the experimental results; however, neglecting concrete confinement as adopted by the American Association of State Highway and Transportation Officials (AASHTO) guidelines[26] showed slightly conservative predictions for the flexural strength of the post-tensioned CFFTs. The average ultimate moment capacity from the experimental test–to–predicted moment capacity ratio M_{uexp}/M_{pred} was 1.05 ± 0.05 with an average coefficient of variation of 4.5% for the partially confined concrete model and 1.11 ± 0.07 with an average coefficient of variation of 6.5% for the unconfined concrete model. Further research is required to investigate additional key parameters affecting the flexural response such as the effect of different types of loading routine, different structural fiber orientations, concrete strengths, and cross-section sizes.
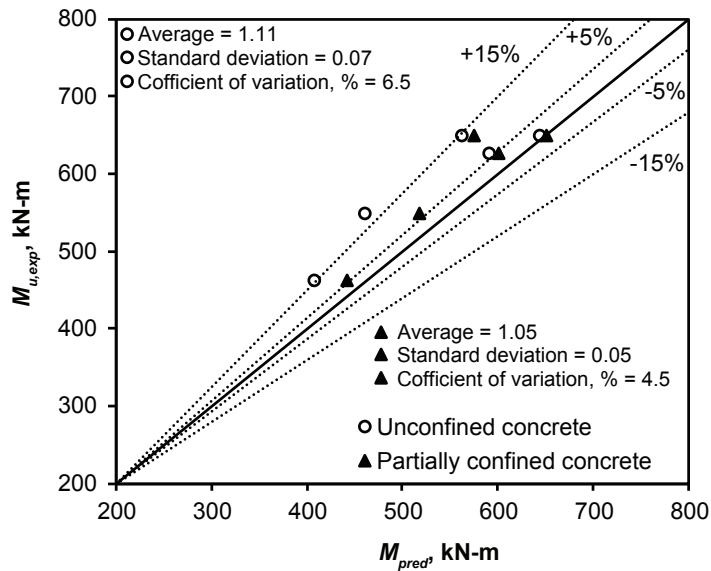
Figure 13. Flexural ultimate moment capacity predictions. Note: M_{pred} = predicated ultimate moment; $M_{u,exp}$ = ultimate moment capacity from experimental test. 1 kN-m = 0.7376 kip-ft.

Conclusion

On the basis of the test results and discussion presented in this study, the following conclusions can be drawn:

- The final failure of the post-tensioned CFFT beams was governed by the rupture of the tube in the tension side, with no evidence of shear failure or web buckling. The post-tensioned CFFT specimens with CFRP laminate showed a progressive failure at a high load level, which can provide a physical warning before final failure.

- For the post-tensioned CFFT beams, the estimated ductility factor λ and energy ratio μ_p values ranged from 8.3 to 10.6 and 82% to 87%, respectively, which indicates ductile flexural behavior.

- The post-tensioned CFFT beams exhibited a nonlinear response with a strength hardening until failure. The degree of nonlinearity strongly depended on the tube structural fiber pattern as well as the bonding of the CFRP laminate embedded in the tension flange.

- Adding CFRP laminates embedded in between the fiber layers of the tension flange of the GFRP tubes could substantially enhance the flexural strength. Post-tensioned CFFT beams with CFRP laminate showed an average 17% increase when compared to post-tensioned CFFT with no CFRP laminate.

- Compared with the specimen with one inclined fiber pattern in hoop direction, the specimen with two inclined fiber patterns exhibited substantially greater postcracking stiffness, ultimate capacity, ductility index, energy absorp-

tion, and reduced deflection at the same load level. The confinement efficiency increased by 48% when the number of inclined fiber patterns was increased from one to two.

- Specimens with the CFRP laminates attached in the bottom flange of the tube achieved flexural strength and energy absorption comparable to the flexural strength and energy absorption of the specimen with two inclined fiber patterns. This finding confirms the efficiency of both systems to enhance both the flexural performance and the strength of the post-tensioned CFFT system. As a result, the design can be optimized to achieve more efficient post-tensioned CFFT structural members.

- A negligible interface slip was observed between the tubes and concrete in most of the post-tensioned CFFTs at both ends up to the peak load. In one specimen, a sudden slip at a high load level occurred at its live end. However, that beam continued to recarry additional loads until it failed in tension at 87% of its peak load. This finding confirms the effectiveness of the system to maintain full composite action between the tube and concrete.

- The predicted values based on the partially confined concrete model show good agreement with the experimental results. Neglecting the concrete confinement as adopted by American Association of State Highway and Transportation Officials (AASHTO) guideline showed slightly conservative predictions for the flexural strength of the post-tensioned CFFTs. The average $M_{u,exp}/M_{pred}$ ratio is 1.05 ± 0.05 with a coefficient of variation of 4.5% for the partially confined model and 1.11 ± 0.07 with a coefficient of variation of 6.5% for the unconfined concrete model.

Acknowledgments

References

1. ASCE (American Society of Civil Engineers). 2021. "2021 Report Card for America's Infrastructure." Accessed March 11, 2022. https://infrastructurereport card.org.

2. Fam, A., and S. K. Mandal. 2006. "Prestressed Concrete–Filled Fiber-Reinforced Polymer Circular Tubes Tested in Flexure." *PCI Journal* 51 (4): 42–54. https://doi .org/10.15554/pcij.07012006.42.54.

3. Ahmed, A., M. Hassan, and R. Masmoudi. 2020. "Effect of Concrete Strength and Tube Thickness on the Flexural Behavior of Prestressed Rectangular Concrete-Filled FRP Tubes Beams." *Engineering Structures Journal* 205: 110112. https://doi.org/10.1016/j.engstruct .2019.110112.

4. Ahmed, A. M. Hassan, and R. Masmoudi. 2020. "Flexural Performance of Unbonded Posttensioned Rectangular Concrete-Filled FRP Tube Beams." *Journal of Composites for Construction* 24 (5). https://doi.org/10.1061 /(ASCE)CC.1943-5614.0001063.

5. Ahmed, A., M. Hassan, and R. Masmoudi. 2021. "Flexural Behavior of Post-Tensioned Normal- and High-Strength Concrete-Filled Fiber-Reinforced Polymer Tubes." *ACI Structural Journal* 118 (2): 73–88. https:// doi.org/10.14359/51728178.

6. ElGawady, M., A. Booker, and H. M. Dawood. 2010. "Seismic Behavior of Posttensioned Concrete-Filled Fiber Tubes." *Journal of Composites for Construction* 14 (5). https://doi.org/10.1061/(ASCE)CC.1943-5614 .0000107.

7. ASTM International. 2018. *Standard Test Method for Compressive Strength of Cylindrical Concrete Specimens*. ASTM C39/C39M-18. West Conshohocken, PA: ASTM International. https://doi.org/10.1520/C0039 _C0039M-18.

8. ASTM International. 2018. *Standard Specification for Deformed and Plain Carbon Steel Bars for Concrete Reinforcement*. ASTM A615/A615M-18e1. West Conshohocken, PA: ASTM International. https://doi.org/10.1520 /A0615_A0615M-18e01.

9. ASTM International. 2017. *Standard Test Method for Tensile Properties of Polymer Matrix Composite Materials*. ASTM D3039/D3039M-17. West Conshohocken, PA: ASTM International. https://doi.org/10.1520/D3039 _D3039M-17.

10. ASTM International. 2015. *Standard Test Method for Compressive Properties of Rigid Plastics*. ASTM D695-15. West Conshohocken, PA: ASTM International. https://doi.org/10.1520/D0695-15.

11. CSA Group. 2014. *Design of Concrete Structures for Buildings*. CSA A23.3 M-14. Rexdale, ON, Canada: CSA Group.

12. Helmi, K., A. Fam, A. Mufti, and J. Hall. 2006. "Effects of Driving Forces and Bending Fatigue on Structural Performance of a Novel Concrete-Filled Fibre-Reinforced-Polymer Tube Flexural Pile." *Canadian Journal of Civil Engineering* 33: 683–691. https://doi.org/10.1139 /l05-075.

13. Abouzied, A., and R. Masmoudi. 2015. "Structural Performance of New Fully and Partially Filled Rectangular FRP-Tube Beams." *Construction and Building Materials* 101 (1): 652–660. https://doi.org/10.1016/j.conbuildmat .2015.10.060.

14. Abouzied, A., and R. Masmoudi. 2017. "Flexural Behavior of Rectangular FRP-Tubes Filled with Reinforced Concrete: Experimental and Theoretical Studies." *Engineering Structures* 133: 59–73. https://doi.org/10.1016/j .engstruct.2016.12.010.

15. Fam, A., D. Schnerch, and S. Rizkalla. 2005. "Rectangular Filament-Wound Glass Fiber Reinforced Polymer Tubes Filled with Concrete under Flexural and Axial Loading: Experimental Investigation." *Journal of Composites for Construction* 9 (1): 25–33. https://doi .org/10.1061/(ASCE)1090-0268(2005)9:1(25).

16. Fam, A., and T. Skutezky. 2006. "Composite T-Beams Using Reduced-Scale Rectangular FRP Tubes and Concrete Slabs." *Journal of Composites for Construction* 10 (2): 172–181. https://doi.org/10.1061/(ASCE)1090 -0268(2006)10:2(172).

17. Fam, A., and S. Rizkalla. 2002. "Flexural Behavior of Concrete-Filled Fiber-Reinforced Polymer Circular Tubes." *Journal of Composites for Construction* 6 (2): 123–132. https://doi.org/10.1061/(ASCE)1090 -0268(2002)6:2(123).

18. Idris, Y., and T. Ozbakkaloglu. (2014). "Flexural Behavior of FRP-HSC-Steel Composite Beams." *Thin-Walled Structures* 80: 207–216. https://doi.org/10.1016/j .tws.2014.03.011.

19. Park, R. 1989. "Evaluation of Ductility of Structures and Structural Assemblages from Laboratory Testing." *Bulletin of the New Zealand National Society for Earthquake Engineering* 22 (3): 155–166. https://doi.org/10.5459/bnzsee.22.3.155-166.

20. Grace, N. F., A. K. Soliman, G. Abdel-Sayed, and K. R. Saleh. 1998. "Behavior and Ductility of Simple and Continuous FRP Reinforced Beams." *Journal of Composites for Construction* 2 (4): 186–194. https://doi.org/10.1061/(ASCE)1090-0268(1998)2:4(186).

21. Naaman, A. E., and S. M. Jeong. 1995. "Structural Ductility of Concrete Beams Prestressed with FRP Tendons." In *Non-metallic (FRP) Reinforcement for Concrete Structures*, edited by L. Taewre, 379–386. New York: CRC Press.

22. Xue, W., Y. Tan, and F. Peng. 2020. "Experimental Study on Damaged Prestressed Concrete Beams Using External Post-Tensioned Tendons." *ACI Structural Journal* 117 (1): 159–168. http://dx.doi.org/10.14359/51718019.

23. Popovics, S. 1973. "A Numerical Approach to the Complete Stress-Strain Curve of Concrete." *Cement and Concrete Research* 3 (5): 583–599. https://doi.org/10.1016/0008-8846(73)90096-3.

24. Fam, A., B. Flisak, and S. Rizkalla. 2003. "Experimental and Analytical Modeling of Concrete-Filled FRP Tubes Subjected to Combined Bending and Axial Loads." *ACI Structural Journal* 100: 499–509.

25. Mattock, A. H. 1979. "Flexural Strength of Prestressed Concrete Section by Programmable Calculator." *PCI Journal* 24 (1): 32–54. https://doi.org/10.15554/pcij.01011979.32.54.

26. AASHTO (American Association of State Highway and Transportation Officials). 2012. *AASHTO LRFD Guide Specifications for Design of Concrete-Filled FRP Tubes for Flexural and Axial Members*. Washington, DC: AASHTO.

Notation

A = constant

A_p = cross-sectional area of prestressing strands

A_s = cross-sectional area of steel bars

B = constant

B_i = inner tube width

c = neutral axis depth

C = constant

$C_{concrete}$ = concrete compression force

$C_{tube,flange}$ = compression force of the tube in the compression flange

$C_{tube,web}$ = compression force of the tube web in the compression zone

e = eccentricity of prestressing tendon

E_{co} = concrete elastic modulus

$E_{elastic}$ = elastic energy absorption

$E_{fc,ave}$ = elastic modulus of tube from compression coupon test

$E_{ft,ave}$ = tensile elastic modulus of tube from tensile coupon test

E_{fu} = modulus of elasticity of the CFRP strips

E_p = elastic modulus of prestressing strand

E_s = elastic modulus of steel bar

E_{sec} = secant modulus of elasticity

E_{tot} = total energy absorption

f_c = concrete strength at any point of the stress-strain curve

f'_c = unconfined compressive strength of concrete cylinder

$f_{fc,ave}$ = compression strength of the tube from compression coupon test

$f_{ft,ave}$ = tensile strength of the tube from tensile coupon test

f_{fu} = ultimate tensile stress of CFRP strips

f_p = prestressing stress

f_{pu} = ultimate prestressing stress

f_{pu} = ultimate stress of prestressing strand

f_{py} = yield tensile stress of strands

f_u = ultimate tensile stress of the steel bars

f_y = yield tensile stress of steel bars

h	= inner tube depth	ε_{cu}	= strain at concrete level
H	= total depth	$\varepsilon_{fc,ave}$	= compression strain of tube from compression coupon test
H_i	= inner tube height	$\varepsilon_{ft,ave}$	= tensile strain of tube from tensile coupon test
M	= external moment	ε_{fu}	= ultimate tensile strain of the CFRP strips
M_{cr}	= cracking moment	ε_p	= strain at the prestressing strand level
M_{pred}	= predicted moment capacity	ε_{pu}	= ultimate strain of prestressing strands
M_u	= ultimate moment	ε_s	= strain in the steel bars
$M_{u,exp}$	= ultimate moment capacity from the experimental test	ε_t	= ultimate strain in tension surface
M_y	= yielding moment	$\varepsilon_{top,tube}$	= strain in the tube top side
N	= external apply forces	$\varepsilon_{tube,bottom}$	= strain in tube at bottom surface
P_{cr}	= cracking load	ε_y	= yielding strain of steel bars
P_{eff}	= effective prestressing forces at transfer	Θ_f	= final slope of the axial-hoop strain curve
P_j	= jacking force	Θ_i	= initial slope of the axial-hoop strain curve
P_u	= peak load	λ	= ductility factor
P_y	= yielding load	μ_p	= energy ratio up to peak load
r	= factor		
t_f	= tube thickness		
T_{Ap}	= force at prestressing strands		
T_{As}	= force at steel bars		
$T_{CFRP,flange}$	= force in the CFRP strips at the tension zone		
$T_{tube,flange}$	= force in the tube flange at the tension zone		
$T_{tube,web}$	= force in the tube web at the tension zone		
Δ_{cr}	= deflection corresponding to cracking load		
Δ_u	= deflection corresponding to ultimate load		
Δ_y	= deflection corresponding to yielding load		
$\varepsilon_{bot,CFRP}$	= strain in the CFRP strip		
$\varepsilon_{bot,tube}$	= strain in the tube bottom side		
ε_c	= strain in the concrete		
ε_c'	= concrete strain at peak load		

About the authors

Asmaa Abdeldaim Ahmed, PhD, is a postdoctoral fellow in the Department of Civil and Building Engineering at the University of Sherbrooke in Sherbrooke, QC, Canada. She received her PhD and MSc in civil engineering from the University of Sherbrooke and her BSc from Helwan University, Cairo, Egypt. Her research interests include structural behavior of concrete-filled, fiber-reinforced polymer tubes and prestressed concrete structures.

Mohamed Hassan, PEng, PhD, is a research associate–lecturer in the Department of Civil and Building Engineering at the University of Sherbrooke and an assistant professor at Helwan University. He received his BSc and MSc in civil engineering from Helwan University and his PhD from the University of Sherbrooke. His research interests include applications of fiber-reinforced polymers in new and innovative construction; rehabilitation of structures; precast, prestressed concrete structures; and large-scale seismic experimental testing.

Radhouane Masmoudi, PEng, PhD, is a professor of civil engineering in the Department of Civil and Building Engineering at the University of Sherbrooke. He received his MSc and PhD from the University of Sherbrooke. He is a voting member of American Concrete Institute (ACI) Committee 440, Fiber Reinforced Polymer Reinforcement, and chair of ACI Committee 440D. His research interests include the development, design, testing, and use of fiber-reinforced polymer reinforcements for concrete and utility applications.

M.-Iqbal Khan, PhD, is a professor of structural engineering in the Department of Civil Engineering and managing director of the Center of Excellence for Concrete Research and Testing at King Saud University in Riyadh, Saudi Arabia. He is an adjunct professor of structural engineering in the Department of Civil, Architectural and Environmental Engineering at the Missouri University of Science and Technology in Rolla.

Abstract

This study extends an extensive research program carried out at the University of Sherbrooke to design and assess the potential use of rectangular, concrete-filled fiber-reinforced-polymer tube (CFFT) beams post-tensioned with steel tendons in bridge applications. This paper describes research to enhance the flexural performance of post-tensioned CFFT beams. Five rectangular post-tensioned CFFT beams were tested up to failure, and the effects of attaching a thin carbon-fiber-reinforced polymer (CFRP) laminate embedded in tension flange and its total reinforcement ratio as well as tube structure fiber laminate were investigated. Last, a simplified design approach is proposed based on strain combinability and force equilibrium to estimate the flexural moment capacity of the tested beams. The specimens with two inclined fiber patterns in the hoop direction or added CFRP laminate strips embedded in the bottom flange of the tubes exhibited substantially greater flexural strength, absorbed energy, and serviceability performance than the control specimens. The ductility index and energy ratio ranged from 8.3 to 10.6 and from 82% to 87%, respectively, which indicates ductile behavior. Also, adding CFRP laminate strips embedded in the bottom flange of the tubes enhanced the flexural strength by 17% on average compared with post-tensioned CFFT without CFRP laminate. The specimen with the CFRP laminates in the bottom flange of the tube achieved flexural strength and energy absorption that was comparable to the flexural strength and energy absorption of the specimen with two layers of inclined fiber patterns. The findings suggest that the design can be optimized to achieve more efficient post-tensioned CFFT structural members. The proposed design approach successfully predicts the flexural strength of the tested beams with an average of 1.05 ± 0.05 for the partially confined concrete model and an average of 1.11 ± 0.07 for the unconfined concrete model.

Keywords

Review policy

This paper was reviewed in accordance with the Precast/Prestressed Concrete Institute's peer-review process. The Precast/Prestressed Concrete Institute is not responsible for statements made by authors of papers in *PCI Journal*. No payment is offered.

Publishing details

Reader comments

Please address any reader comments to *PCI Journal* editor-in-chief Tom Klemens at tklemens@pci.org or Precast/Prestressed Concrete Institute, c/o *PCI Journal*, 8770 W. Bryn Mawr Ave., Suite 1150, Chicago, IL 60631. ∎